

# The long-distance window of the hadronic vacuum polarization for the muon $g - 2$

T. Blum,<sup>1</sup> P. A. Boyle,<sup>2,3</sup> M. Bruno,<sup>4,5</sup> B. Chakraborty,<sup>6</sup> F. Erben,<sup>7</sup> V. Gülpers,<sup>3</sup>  
 A. Hackl,<sup>8</sup> N. Hermansson-Truedsson,<sup>3</sup> R. C. Hill,<sup>3</sup> T. Izubuchi,<sup>2,9</sup> L. Jin,<sup>1</sup> C. Jung,<sup>2</sup>  
 C. Lehner,<sup>8,\*</sup> J. McKeon,<sup>6</sup> A. S. Meyer,<sup>10</sup> M. Tomii,<sup>1,9</sup> J. T. Tsang,<sup>7</sup> and X.-Y. Tuo<sup>2</sup>

(RBC and UKQCD Collaborations)

<sup>1</sup>*Physics Department, University of Connecticut, Storrs, CT 06269-3046, USA*

<sup>2</sup>*Physics Department, Brookhaven National Laboratory, Upton, NY 11973, USA*

<sup>3</sup>*School of Physics and Astronomy, The University of Edinburgh, Edinburgh EH9 3FD, UK*

<sup>4</sup>*Dipartimento di Fisica, Università di Milano-Bicocca, Piazza della Scienza 3, I-20126 Milano, Italy*

<sup>5</sup>*INFN, Sezione di Milano-Bicocca, Piazza della Scienza 3, I-20126 Milano, Italy*

<sup>6</sup>*School of Physics and Astronomy, University of Southampton, Southampton SO17 1BJ, UK*

<sup>7</sup>*CERN, Theoretical Physics Department, Geneva, Switzerland*

<sup>8</sup>*Fakultät für Physik, Universität Regensburg, Universitätsstraße 31, 93040 Regensburg, Germany*

<sup>9</sup>*RIKEN-BNL Research Center, Brookhaven National Laboratory, Upton, NY 11973, USA*

<sup>10</sup>*Nuclear and Chemical Sciences Division, Lawrence Livermore National Laboratory, Livermore, CA 94550, USA*

(Dated: October 29, 2024)

We provide the first ab-initio calculation of the Euclidean long-distance window of the isospin symmetric light-quark connected contribution to the hadronic vacuum polarization for the muon  $g - 2$  and find  $a_\mu^{\text{LD,iso,conn,ud}} = 411.4(4.3)(2.4) \times 10^{-10}$ . We also provide the currently most precise calculation of the total isospin symmetric light-quark connected contribution,  $a_\mu^{\text{iso,conn,ud}} = 666.2(4.3)(2.5) \times 10^{-10}$ , which is more than  $4\sigma$  larger compared to the data-driven estimates of Boito et al. 2022 and  $1.7\sigma$  larger compared to the lattice QCD result of BMW20.

PACS numbers: 12.38.Gc

## INTRODUCTION

The relative deviation of the muon's Landé factor  $g_\mu$  from Dirac's relativistic quantum mechanics result,  $a_\mu = (g_\mu - 2)/2$ , also called the anomalous magnetic moment of the muon, is one of the most precisely determined quantities in particle physics. It is sensitive to virtual contributions of particles which may be out of reach of direct production in high-energy experiments and it therefore plays an important role in constraining new physics. Substantial efforts have been undertaken at Fermilab (E989) and are planned at J-PARC (E34) [1] in order to further improve the precision of the experimental determination. In 2021 the Fermilab experiment released first results [2] which confirmed the previously best result obtained by the BNL E821 experiment [3] and reduced the experimental uncertainty from 0.54 ppm to 0.46 ppm. Subsequently they released results for runs II and III in 2023 which yielded an uncertainty of 0.2 ppm [4]. In 2025 the Fermilab experiment aims to release their final results pushing the uncertainty down to approximately 0.14 ppm [5].

Matching the precision of this spectacular experimental result in a theory calculation of the Standard Model (SM) contribution to  $a_\mu$  is a substantial challenge and is currently a work in progress. In 2020 the Muon  $g-2$  Theory Initiative published a whitepaper [6–26] which indicated a more than  $4\sigma$  tension of the experimental result with the SM. This result relied on a data-driven estimate of the hadronic vacuum polarization (HVP) contribution

based on  $e^+e^- \rightarrow$  hadron experimental data. While existing tensions between experimental data sets had been taken into account in 2020 by inflating the uncertainties appropriately, the recent result by CMD-3 [27, 28] increases the tensions to a degree that currently appears to make a data-driven high-precision evaluation of the HVP not feasible.

At the same time, lattice methodology is maturing and is on track to allow for a complete ab-initio theory determination that soon may match the Fermilab E989 target precision. In this context, it is now common practice to separate the total HVP contribution into the Euclidean windows introduced in our previous work [29], which separate three different regions (short-distance, intermediate-distance, long-distance) that exactly sum up to the total HVP. Each region has its own dominant challenges that can best be addressed by targeted calculations optimized separately for each region.

The short-distance region suffers from large discretization errors and very fine lattices are needed. The intermediate-distance region has moderate uncertainties. The long-distance region suffers from large statistical and finite-size errors. For lattice calculations using rooted staggered quarks additional challenges for the continuum limit of the long-distance contribution exist, see, e.g. Ref. [30].

By now there is very good agreement among several lattice collaborations on the short-distance and intermediate-distance windows [30–42]. The same consolidation at high precision is also needed for the long-

distance region, and the current paper which focuses on the dominant light-quark connected contribution is a first step in this direction. The results reported in the following are unchanged compared to our unblinding presentation at Lattice 2024 [43].

In future work, we will improve our previous results [29] on the quark disconnected contributions, strong-isospin-breaking (SIB) and QED corrections and improve our lattice spacing determinations to complete the calculation of  $a_\mu$  at the next precision frontier. We note that a combination of lattice and data-driven methodology is also an interesting approach as suggested in Ref. [29] and recently demonstrated in Ref. [40].

## METHODOLOGY

We address the particular challenges of the long-distance window by building on ideas of the improved bounding method [44] and finite-volume exclusive state reconstruction [45]. These methods are expressed in terms of the time-momentum representation [46]

$$a_\mu^{\text{HVP LO}} = \sum_{t=0}^{\infty} w_t C(t) \quad (1)$$

with  $C(t) = \frac{1}{3} \sum_{\vec{x}} \sum_{j=0,1,2} \langle J_j(\vec{x}, t) J_j(0) \rangle$ , vector current  $J_\mu(x) = i \sum_f Q_f \bar{\Psi}_f(x) \gamma_\mu \Psi_f(x)$  with fractional electric charge  $Q_f$ , and sum over quark flavors  $f$ . The correlator  $C(t)$  at zero temperature admits a spectral representation

$$C(t) = \frac{1}{3} \sum_{j=0,1,2} \sum_n |\langle n | \hat{J}_j | 0 \rangle|^2 e^{-E_n t} \quad (2)$$

with zero-momentum vector operator  $\hat{J}_j$ , Hamiltonian eigenstate  $|n\rangle$ , and energy  $E_n$  for the discrete finite-volume spectrum. The weights  $w_t$  can be discretized in different ways. We use the two approaches described in Ref. [31]. We drop the HVP LO label in the following and separate the window contributions as in Ref. [29] into  $a_\mu = a_\mu^{\text{SD}} + a_\mu^{\text{W}} + a_\mu^{\text{LD}}$ . We have  $a_\mu^{\text{SD}}(t_0, \Delta) = \sum_{t=0}^{\infty} C(t) w_t [1 - \Theta(t, t_0, \Delta)]$ ,  $a_\mu^{\text{W}}(t_0, t_1, \Delta) = \sum_{t=0}^{\infty} C(t) w_t [\Theta(t, t_0, \Delta) - \Theta(t, t_1, \Delta)]$ , and  $a_\mu^{\text{LD}}(t_1, \Delta) = \sum_{t=0}^{\infty} C(t) w_t \Theta(t, t_1, \Delta)$  with  $\Theta(t, t', \Delta) = [1 + \tanh[(t - t')/\Delta]]/2$ . We select  $t_0 = 0.4$  fm,  $t_1 = 1.0$  fm, and  $\Delta = 0.15$  fm as suggested in Ref. [29].

The correlators  $C(t)$  are computed with a hierarchical approximation scheme [29, 47, 48] using locally-coherent low-modes with exact eigenvalues [49]. In addition, as described in Ref. [44], we use exact distillation [50, 51] and have made our code publicly available [52].

In Tab. I we provide a list of all lattice gauge ensembles used in this study. For the physical pion mass ensembles with  $m_\pi L \approx 5$  (96I and C) we use 200 Laplace

ID	$a^{-1}/\text{GeV}$	$L^3 \times T \times L_s/a^5$	$m_\pi/\text{MeV}$	$m_K/\text{MeV}$	$m_\pi L$
96I	2.6920(67)	$96^3 \times 192 \times 12$	131.29(66)	484.5(2.3)	4.7
64I	2.3549(49)	$64^3 \times 128 \times 12$	138.98(43)	507.5(1.5)	3.8
48I	1.7312(28)	$48^3 \times 96 \times 24$	139.32(30)	499.44(88)	3.9
C	1.7312(28)	$64^3 \times 96 \times 24$	139.32(30)	499.44(88)	5.2
4	1.7312(28)	$24^3 \times 48 \times 24$	274.8(2.5)	530.1(3.1)	3.8
D	1.7312(28)	$32^3 \times 48 \times 24$	274.8(2.5)	530.1(3.1)	3.8
1	1.7312(28)	$32^3 \times 64 \times 24$	208.1(1.1)	514.0(1.8)	3.8
3	1.7312(28)	$32^3 \times 64 \times 24$	211.3(2.3)	603.8(6.1)	3.9
9	2.3549(49)	$32^3 \times 64 \times 12$	278.9(0.6)	531.2(0.7)	3.8
L	2.3549(49)	$64^3 \times 128 \times 12$	278.9(0.6)	531.2(0.7)	7.6

TABLE I. List of  $N_f = 2 + 1$  ensembles with parameters determined in the RBC/UKQCD18 isospin symmetric world defined in Eq. 3. The ensembles have Iwasaki gauge action and Möbius [53] domain-wall [54, 55] fermion sea quarks with  $b = 1.5$  and  $c = 0.5$ . The parameters  $b$  and  $c$  are defined in Ref. [56]. The scripts generating the new ensembles are publicly available [52].

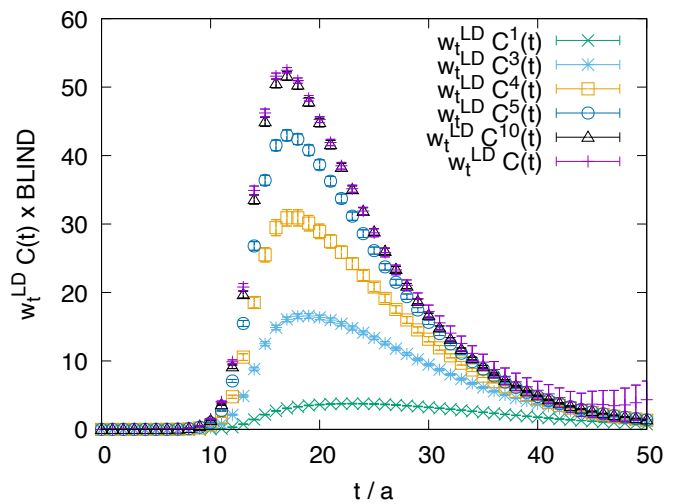


FIG. 1. Reconstruction of the lowest  $N$  states  $C^N(t)$  compared to the inclusive  $C(t)$  for the 96I ensemble with  $w_t^{\text{LD}} = w_t \Theta(t, t_1, \Delta)$ . The exponential growth of statistical noise in  $C(t)$  is absent in the reconstruction.

eigenmodes and for all other ensembles we use 60. We use an operator basis including a local vector current, a distillation-smeared vector current, and two-pion operators up to a relative momentum of  $p = (2, 0, 0)(2\pi/L)$  for the case of 60 Laplace eigenmodes and  $p = (2, 2, 0)(2\pi/L)$  for the case of 200 Laplace eigenmodes. All operators are in the  $T_1^u, I = 1$  irreducible representation since we focus on the dominant light-quark connected contribution.

In Fig. 1, we demonstrate the reconstruction of the first  $N$  states via  $C^N(t) = (1/3) \sum_{j=0,1,2} \sum_{n=1}^N |\langle n | \hat{J}_j | 0 \rangle|^2 e^{-E_n t}$  compared to the full  $C(t)$ . The figure shows the result of using only distillation smeared operators (vector and two-pion) in a generalized eigenvalue problem (GEVP) study [57, 58] to find the  $E_n$  and optimal operators to project

to a given state  $|n\rangle$ . This operator is contracted with the local vector current to obtain the overlap factor  $|\langle n|\hat{J}_j|0\rangle|^2$ . The reconstruction  $C^N(t)$  is used at large Euclidean times  $t$ , where  $C^N(t) = C(t)$  within statistical uncertainties.

As in our previous work [31], we perform the analysis in a blinded manner with five analysis groups A-E. Four analysis groups A-D have conducted a full analysis, while one group (E) has focused on cross-checks. Each analysis group received the correlator data with a blinding factor applied to each insertion of a local vector current. The blinding factor was unique to each group and generated using a hash function based on the group's name (A-E). The blinding factors were applied by a script, and no one in the collaboration saw the blinding factors themselves. The process was managed by one of the authors (CL). Once the analysis groups were ready, relative unblinding meetings between two analysis groups were organized in which the respective methods were scrutinized. After conclusion of this process the relative blinding factor was removed between the participating groups. After the relative unblinding, the collaboration agreed to the RBC/UKQCD24 prescription for the analysis that will be described in detail in the following. This procedure was then applied to a final analysis before the absolute blinding was removed in a joint meeting on July 19, 2024. The cross-checks of group E were conducted prior to the unblinding and focused on results that were not affected by the blinding factor such as the ratio of  $C^N(t)$  to  $C(t)$  for which the blinding factor drops out, as well as checks of individual  $E_n$  that are also not affected by the blinding. Additional details on the cross-checks and on the various methods studied by the individual groups are provided as supplemental material to this letter.

The calculation of  $C(t)$  is organized as an expansion around an isospin-symmetric point [29, 59–63]. In this work, we provide results for two choices of the expansion point, following our earlier work [31]. The first choice is the RBC/UKQCD18 world defined by

$$\begin{aligned} m_\pi &= 0.135 \text{ GeV}, & m_K &= 0.4957 \text{ GeV}, \\ m_\Omega &= 1.67225 \text{ GeV}, \end{aligned} \quad (3)$$

consistent with Ref. [29]. We also consider a second choice

$$\begin{aligned} m_\pi &= 0.13497 \text{ GeV}, & m_{ss^*} &= 0.6898 \text{ GeV}, \\ w_0 &= 0.17236 \text{ fm}, \end{aligned} \quad (4)$$

which we label as the BMW20 world [30]. We define  $m_{ss^*}$  as the ground-state energy of the quark-connected pseudoscalar  $\bar{s}s$  meson two-point function. To avoid an unnecessary inflation of uncertainties when comparing isospin-symmetric lattice results, we define the above values without uncertainties. The experimental uncertainties of the physical hadron spectrum enter when QED and SIB corrections are included.

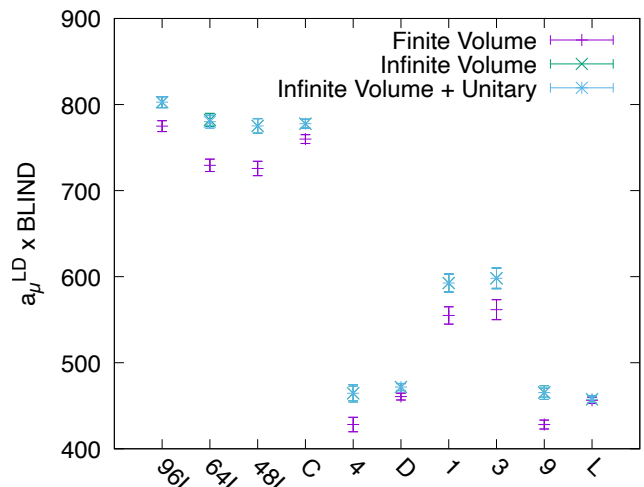


FIG. 2. Results for the ensembles listed in Tab. I with and without finite-volume corrections applied. For ensemble 64I a small correction from the partially-quenched point to the unitary point is added as well, see Ref. [31].

Finite-volume corrections are applied using the Hansen-Patella formalism [64, 65] in the monopole approximation. As can be seen in Fig. 2, after applying finite-volume corrections the results for ensembles that only differ by the lattice volume (4 and D, 9 and L, 48I and C) agree within uncertainties. We provide a detailed study of the agreement as a function of Euclidean time in the supplemental material. It is noteworthy that for our largest volume with  $m_\pi L = 7.6$  (L), the finite-volume corrections are smaller than the quoted statistical uncertainties.

## ANALYSIS AND RESULTS

In the following, we describe the RBC/UKQCD24 prescription for determining the light-quark connected contribution to the long-distance window in the isospin symmetric limit,  $a_\mu^{\text{LD,iso,conn,ud}}$ .

For each ensemble in Tab. I, the long-distance part of  $C(t)$  is replaced by  $C^N(t)$  for sufficiently large times such that they agree within statistical uncertainties. For the ensembles with 200 Laplace modes  $N = 10$  and for all other ensembles  $N = 5$ . In all cases this allows for a spectral reconstruction beyond the peak of the rho resonance. Finite-volume corrections are applied as shown in Fig. 2. These data points are fit jointly to several fit functions. We study both an additive and a multiplicative combination of discretization and mass-mistuning effects

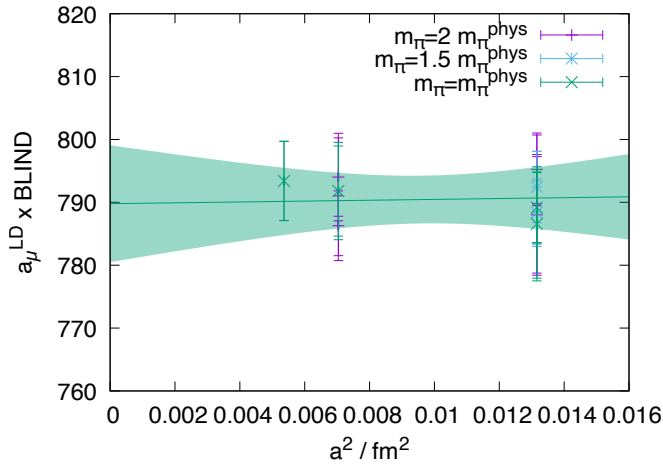


FIG. 3. Fit result of  $f_*$  with  $Z_V^\pi$  and without setting  $f_3 = 0$ . The data is shown for all ensembles as a function of  $a^2$  after subtracting the fit function without the  $f_0 f_1 a^2$  term.

by varying between

$$f_+ = f_0 + f_1 a^2 + f_2 (w_0 m_\pi - (w_0 m_\pi)_{\text{phys}}) + f_3 (w_0 m_\pi - (w_0 m_\pi)_{\text{phys}})^2 + f_4 (w_0 m_{ss*} - (w_0 m_{ss*})_{\text{phys}}) \quad (5)$$

and

$$f_* = f_0 (1 + f_1 a^2) (1 + f_2 (w_0 m_\pi - (w_0 m_\pi)_{\text{phys}}) + f_3 (w_0 m_\pi - (w_0 m_\pi)_{\text{phys}})^2 + f_4 (w_0 m_{ss*} - (w_0 m_{ss*})_{\text{phys}})). \quad (6)$$

The functional forms as given apply to the BMW20 world and the dimensionless ratios  $w_0 m_\pi$  and  $w_0 m_{ss*}$  have to be replaced with  $m_\pi/m_\Omega$  and  $m_K/m_\Omega$  for the RBC/UKQCD18 world. For both fit functions, we also study versions with  $f_3 = 0$ . These four fit forms are then applied to the data renormalized with two different choices for the local vector current renormalization constant:  $Z_V^\pi$  and  $Z_V^*$ . The former is defined by the pion charge, the latter by the ratio of local-conserved to local-local correlators at a distance of 1 fm. This results in 8 fits that are then combined in a model average. All fit forms have acceptable  $p$ -value and the results are consistent between using the Akaike information criterion (AIC) [66], a simple  $\chi^2$  weight, and a flat weight of all models. We provide individual results in the supplemental material. We also studied more divergent chiral dependencies, however, since our analysis is dominated by four ensembles at physical pion mass, such variations have little impact on the fit results. In Fig. 3, we show the fit result of  $f_*$  with  $Z_V^\pi$  and without setting  $f_3 = 0$ . We emphasize that the extrapolation to the continuum limit is within the statistical uncertainties of the finest data point.

In Fig. 4, we compare the results obtained by the different analysis groups to the RBC/UKQCD24 prescription.

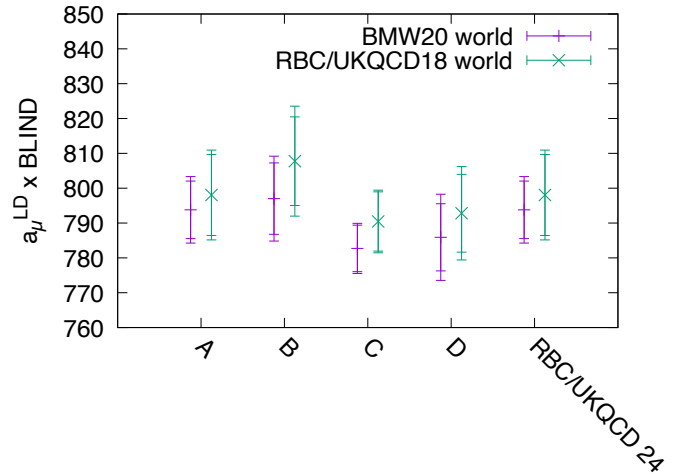


FIG. 4. Results obtained by the different analysis groups and the resulting RBC/UKQCD24 prescription.

We observed good agreement prior to the absolute blinding and have identified the reasons for the residual variations. We note that group D only took the continuum limit of physical pion mass ensembles. Groups A and B also verified the consistency of the continuum limits with and without ensembles 9 and L. The lattice spacing uncertainty due to our more limited knowledge of the  $\Omega^-$  mass is responsible for the larger errors in RBC/UKQCD18 world. Work on a more precise determination of  $m_\Omega$  is in progress. We observe that RBC/UKQCD18 and BMW20 worlds are consistent at the current precision.

Our final results are

$$a_\mu^{\text{LD,iso,conn,ud}} = 411.4(4.3)(2.4) \times 10^{-10}, \quad a_\mu^{\text{iso,conn,ud}} = 666.2(4.3)(2.5) \times 10^{-10} \quad (7)$$

in the BMW20 world and

$$a_\mu^{\text{LD,iso,conn,ud}} = 413.6(6.0)(2.9) \times 10^{-10}, \quad a_\mu^{\text{iso,conn,ud}} = 668.7(6.1)(2.9) \times 10^{-10} \quad (8)$$

in the RBC/UKQCD18 world, where the first error is statistical and the second systematic. The total isospin symmetric results are obtained by adding our previous short-distance and intermediate-distance results [31].

In Fig. 5, we compare our results in the BMW20 world to the literature [74]. Our result for  $a_\mu^{\text{iso,conn,ud}}$  is more than  $4\sigma$  larger compared to the data-driven estimates by Boito, *et al.* 2022 [73] which were obtained based on the data sets that entered the Theory Initiative whitepaper [6] prior to the release of the CMD-3 data. This observed shift with respect to the data-driven estimate is consistent with the size of the tension between experiment and theory for the muon  $g-2$  quoted in the 2020 whitepaper of the Muon  $g-2$  Theory Initiative [6]. Finally, we note that our result is also  $1.7\sigma$  larger compared to the lattice QCD result of BMW20 [30].

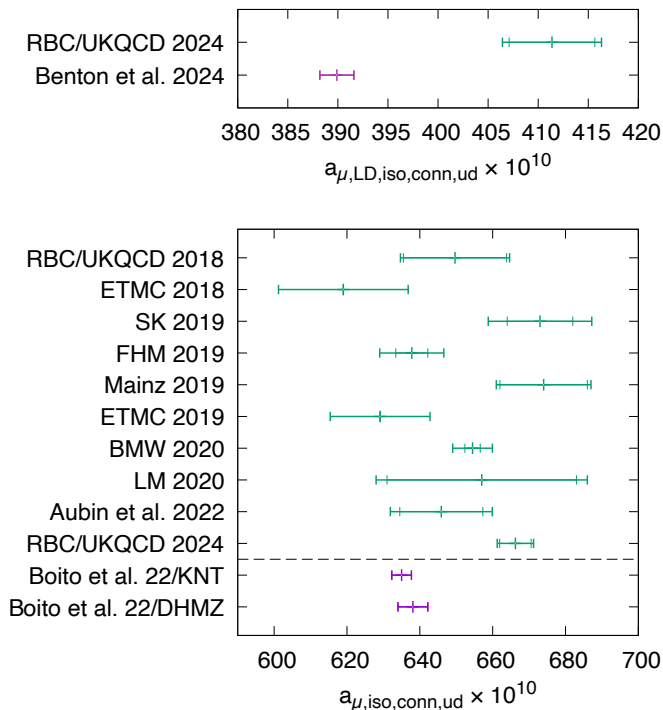


FIG. 5. This work compared to the literature: Benton et al. 2024 [67], RBC/UKQCD 2018 [29], ETMC 2018 [68], SK 2019 [69], FHM 2019 [70], Mainz 2019 [71], ETMC 2019 [72], BMW 2020 [30], LM 2020 [34], Aubin et al. 2022 [35], and Boito et al. 2022/KNT and Boito et al. 2022/DHMZ [73].

## CONCLUSIONS AND OUTLOOK

In this work we compute the long-distance Euclidean window of the hadronic vacuum polarization for light quarks in the isospin symmetric limit. This calculation is particularly challenging and dominates the total uncertainty of a complete high-precision  $a_{\mu}^{\text{HVP LO}}$  result obtained from first-principles lattice QCD methods. All calculations were performed in a blinded manner. We find a large tension with the data-driven approach [73] based on data sets that were also used in Ref. [6] but also a smaller tension with the BMW20 result [30]. More work is needed to complete an ab-initio calculation matching the Fermilab E989 target precision. We are currently improving our previous estimates for the quark-disconnected contributions and the QED and SIB corrections including diagrams beyond the electro-quenched approximation. We expect to match the FNAL E989 target precision upon completion of our HVP program.

## ACKNOWLEDGMENTS

We thank our colleagues of the RBC and UKQCD collaborations for many valuable discussions and joint efforts over the years. The authors gratefully ac-

knowledge the Gauss Centre for Supercomputing e.V. ([www.gauss-centre.eu](http://www.gauss-centre.eu)) for funding this project by providing computing time on the GCS Supercomputer JUWELS at Jülich Supercomputing Centre (JSC). We acknowledge the EuroHPC Joint Undertaking for awarding this project access to the EuroHPC supercomputer LUMI, hosted by CSC (Finland) and the LUMI consortium through a EuroHPC Extreme Scale Access call as well as the EuroHPC supercomputer LEONARDO, hosted by CINECA (Italy). An award of computer time was provided by the ASCR Leadership Computing Challenge (ALCC) and Innovative and Novel Computational Impact on Theory and Experiment (INCITE) programs. This research used resources of the Argonne Leadership Computing Facility, which is a DOE Office of Science User Facility supported under contract DE-AC02-06CH11357. This research also used resources of the Oak Ridge Leadership Computing Facility, which is a DOE Office of Science User Facility supported under Contract DE-AC05-00OR22725. This research used resources of the National Energy Research Scientific Computing Center (NERSC), a U.S. Department of Energy Office of Science User Facility located at Lawrence Berkeley National Laboratory, operated under Contract No. DE-AC02-05CH11231 using NERSC award NESAP m1759 for 2020. This work used the DiRAC Blue Gene Q Shared Petaflop system at the University of Edinburgh, operated by the Edinburgh Parallel Computing Centre on behalf of the STFC DiRAC HPC Facility ([www.dirac.ac.uk](http://www.dirac.ac.uk)). This equipment was funded by BIS National E-infrastructure capital grant ST/K000411/1, STFC capital grant ST/H008845/1, and STFC DiRAC Operations grants ST/K005804/1 and ST/K005790/1. DiRAC is part of the National E-Infrastructure. We gratefully acknowledge disk and tape storage provided by USQCD and by the University of Regensburg with support from the DFG. The lattice data analyzed in this project was generated using GPT [52], Grid [75], and CPS [76] and analyzed, in part, using pyobs [77]. TB is supported by the US DOE under grant DE-SC0010339. PB, TI, and CJ were supported in part by US DOE Contract DESC0012704(BNL) and the Scientific Discovery through Advanced Computing (SciDAC) program LAB 22-2580. At the beginning of the project, MB was supported by the national program for young researchers “Rita Levi Montalcini”. MB is (partially) supported by ICSC - Centro Nazionale di Ricerca in High Performance Computing, Big Data and Quantum Computing, funded by European Union – NextGenerationEU. Research of BC at the University of Southampton has been supported by the following research fellowship and grants - Leverhulme Trust (ECF-2019-223 G100820), STFC (Grant no. ST/X000583/1), STFC (Grant no. ST/W006251/1), and EPSRC (Grant no. EP/W032635/1). FE has received funding from the European Union’s Horizon Europe research and innovation programme under the Marie



Skłodowska-Curie grant agreement No. 101106913. VG is supported in part by UK STFC grant ST/P000630/1, ST/T000600/1 and ST/X000494/1. AH is supported by the Hans-Böckler-Stiftung. NHT is funded by the UK Research and Innovation, Engineering and Physical Sciences Research Council, grant number EP/X021971/1. RH is supported by UK STFC Grant No. ST/P000630/1. TI is also supported by the Department of Energy, Laboratory Directed Research and Development (LDRD No. 23-051) of BNL and RIKEN BNL Research Center. LJ and MT acknowledge the support of DOE Office of Science Early Career Award DE-SC0021147 and DOE grant DE-SC0010339. ASM is supported in part by Lawrence Livermore National Security, LLC #DE-AC52-07NA27344, Neutrino Theory Network Program Grant #DE-AC02-07CHI11359, and the U.S. Department of Energy Award #DE-SC0020250. XYT has been supported by US DOE Contract DESC0012704(BNL).

---

\* Corresponding author; christoph.lehner@ur.de

- [1] M. Abe *et al.*, A New Approach for Measuring the Muon Anomalous Magnetic Moment and Electric Dipole Moment, *PTEP* **2019**, 053C02 (2019), arXiv:1901.03047 [physics.ins-det].
- [2] B. Abi *et al.* (Muon  $g-2$ ), Measurement of the Positive Muon Anomalous Magnetic Moment to 0.46 ppm, *Phys. Rev. Lett.* **126**, 141801 (2021), arXiv:2104.03281 [hep-ex].
- [3] G. Bennett *et al.* (Muon  $G-2$ ), Final Report of the Muon E821 Anomalous Magnetic Moment Measurement at BNL, *Phys.Rev.* **D73**, 072003 (2006), arXiv:hep-ex/0602035 [hep-ex].
- [4] D. P. Aguillard *et al.* (Muon  $g-2$ ), Measurement of the Positive Muon Anomalous Magnetic Moment to 0.20 ppm, *Phys. Rev. Lett.* **131**, 161802 (2023), arXiv:2308.06230 [hep-ex].
- [5] R. Carey, K. Lynch, J. Miller, B. Roberts, W. Morse, *et al.*, The New ( $g-2$ ) Experiment: A proposal to measure the muon anomalous magnetic moment to  $\pm 0.14$  ppm precision (2009).
- [6] T. Aoyama *et al.*, The anomalous magnetic moment of the muon in the Standard Model, *Phys. Rept.* **887**, 1 (2020), arXiv:2006.04822 [hep-ph].
- [7] T. Aoyama, M. Hayakawa, T. Kinoshita, and M. Nio, Complete Tenth-Order QED Contribution to the Muon  $g - 2$ , *Phys. Rev. Lett.* **109**, 111808 (2012), arXiv:1205.5370 [hep-ph].
- [8] T. Aoyama, T. Kinoshita, and M. Nio, Theory of the Anomalous Magnetic Moment of the Electron, *Atoms* **7**, 28 (2019).
- [9] A. Czarnecki, W. J. Marciano, and A. Vainshtein, Refinements in electroweak contributions to the muon anomalous magnetic moment, *Phys. Rev.* **D67**, 073006 (2003), [Erratum: *Phys. Rev.* **D73**, 119901 (2006)], arXiv:hep-ph/0212229 [hep-ph].
- [10] C. Gnendiger, D. Stöckinger, and H. Stöckinger-Kim, The electroweak contributions to  $(g - 2)_\mu$  after the Higgs boson mass measurement, *Phys. Rev.* **D88**, 053005 (2013), arXiv:1306.5546 [hep-ph].
- [11] M. Davier, A. Hoecker, B. Malaescu, and Z. Zhang, Reevaluation of the hadronic vacuum polarisation contributions to the Standard Model predictions of the muon  $g-2$  and  $\alpha(m_Z^2)$  using newest hadronic cross-section data, *Eur. Phys. J.* **C77**, 827 (2017), arXiv:1706.09436 [hep-ph].
- [12] A. Keshavarzi, D. Nomura, and T. Teubner, Muon  $g - 2$  and  $\alpha(M_Z^2)$ : a new data-based analysis, *Phys. Rev.* **D97**, 114025 (2018), arXiv:1802.02995 [hep-ph].
- [13] G. Colangelo, M. Hoferichter, and P. Stoffer, Two-pion contribution to hadronic vacuum polarization, *JHEP* **02**, 006, arXiv:1810.00007 [hep-ph].
- [14] M. Hoferichter, B.-L. Hoid, and B. Kubis, Three-pion contribution to hadronic vacuum polarization, *JHEP* **08**, 137, arXiv:1907.01556 [hep-ph].
- [15] M. Davier, A. Hoecker, B. Malaescu, and Z. Zhang, A new evaluation of the hadronic vacuum polarisation contributions to the muon anomalous magnetic moment and to  $\alpha(m_Z^2)$ , *Eur. Phys. J.* **C80**, 241 (2020), [Erratum: *Eur. Phys. J.* **C80**, 410 (2020)], arXiv:1908.00921 [hep-ph].
- [16] A. Keshavarzi, D. Nomura, and T. Teubner, The  $g - 2$  of charged leptons,  $\alpha(M_Z^2)$  and the hyperfine splitting of muonium, *Phys. Rev.* **D101**, 014029 (2020), arXiv:1911.00367 [hep-ph].
- [17] A. Kurz, T. Liu, P. Marquard, and M. Steinhauser, Hadronic contribution to the muon anomalous magnetic moment to next-to-next-to-leading order, *Phys. Lett.* **B734**, 144 (2014), arXiv:1403.6400 [hep-ph].
- [18] K. Melnikov and A. Vainshtein, Hadronic light-by-light scattering contribution to the muon anomalous magnetic moment revisited, *Phys. Rev.* **D70**, 113006 (2004), arXiv:hep-ph/0312226 [hep-ph].
- [19] P. Masjuan and P. Sánchez-Puertas, Pseudoscalar-pole contribution to the  $(g_\mu - 2)$ : a rational approach, *Phys. Rev.* **D95**, 054026 (2017), arXiv:1701.05829 [hep-ph].
- [20] G. Colangelo, M. Hoferichter, M. Procura, and P. Stoffer, Dispersion relation for hadronic light-by-light scattering: two-pion contributions, *JHEP* **04**, 161, arXiv:1702.07347 [hep-ph].
- [21] M. Hoferichter, B.-L. Hoid, B. Kubis, S. Leupold, and S. P. Schneider, Dispersion relation for hadronic light-by-light scattering: pion pole, *JHEP* **10**, 141, arXiv:1808.04823 [hep-ph].
- [22] A. Gérardin, H. B. Meyer, and A. Nyffeler, Lattice calculation of the pion transition form factor with  $N_f = 2 + 1$  Wilson quarks, *Phys. Rev.* **D100**, 034520 (2019), arXiv:1903.09471 [hep-lat].
- [23] J. Bijnens, N. Hermansson-Truedsson, and A. Rodríguez-Sánchez, Short-distance constraints for the HLbL contribution to the muon anomalous magnetic moment, *Phys. Lett.* **B798**, 134994 (2019), arXiv:1908.03331 [hep-ph].
- [24] G. Colangelo, F. Hagelstein, M. Hoferichter, L. Laub, and P. Stoffer, Longitudinal short-distance constraints for the hadronic light-by-light contribution to  $(g-2)_\mu$  with large- $N_c$  Regge models, *JHEP* **03**, 101, arXiv:1910.13432 [hep-ph].
- [25] T. Blum, N. Christ, M. Hayakawa, T. Izubuchi, L. Jin, C. Jung, and C. Lehner, The hadronic light-by-light scattering contribution to the muon anomalous magnetic moment from lattice QCD, *Phys. Rev. Lett.* **124**, 132002 (2020), arXiv:1911.08123 [hep-lat].
- [26] G. Colangelo, M. Hoferichter, A. Nyffeler, M. Passera, and P. Stoffer, Remarks on higher-order hadronic correc-

- tions to the muon  $g - 2$ , Phys. Lett. **B735**, 90 (2014), arXiv:1403.7512 [hep-ph].
- [27] F. V. Ignatov *et al.* (CMD-3), Measurement of the Pion Form Factor with CMD-3 Detector and its Implication to the Hadronic Contribution to Muon ( $g-2$ ), Phys. Rev. Lett. **132**, 231903 (2024), arXiv:2309.12910 [hep-ex].
- [28] F. V. Ignatov *et al.* (CMD-3), Measurement of the  $e+e-\rightarrow\pi+\pi-$  cross section from threshold to 1.2 GeV with the CMD-3 detector, Phys. Rev. D **109**, 112002 (2024), arXiv:2302.08834 [hep-ex].
- [29] T. Blum, P. A. Boyle, V. Gülpers, T. Izubuchi, L. Jin, C. Jung, A. Jüttner, C. Lehner, A. Portelli, and J. T. Tsang (RBC, UKQCD), Calculation of the hadronic vacuum polarization contribution to the muon anomalous magnetic moment, Phys. Rev. Lett. **121**, 022003 (2018), arXiv:1801.07224 [hep-lat].
- [30] S. Borsanyi *et al.*, Leading hadronic contribution to the muon magnetic moment from lattice QCD, Nature **593**, 51 (2021), arXiv:2002.12347 [hep-lat].
- [31] T. Blum *et al.* (RBC, UKQCD), Update of Euclidean windows of the hadronic vacuum polarization, Phys. Rev. D **108**, 054507 (2023), arXiv:2301.08696 [hep-lat].
- [32] C. Aubin, T. Blum, C. Tu, M. Golterman, C. Jung, and S. Peris, Light quark vacuum polarization at the physical point and contribution to the muon  $g - 2$ , Phys. Rev. D **101**, 014503 (2020), arXiv:1905.09307 [hep-lat].
- [33] D. Giusti and S. Simula, Window contributions to the muon hadronic vacuum polarization with twisted-mass fermions, PoS **LATTICE2021**, 189 (2022), arXiv:2111.15329 [hep-lat].
- [34] C. Lehner and A. S. Meyer, Consistency of hadronic vacuum polarization between lattice QCD and the R-ratio, Phys. Rev. D **101**, 074515 (2020), arXiv:2003.04177 [hep-lat].
- [35] C. Aubin, T. Blum, M. Golterman, and S. Peris, Muon anomalous magnetic moment with staggered fermions: Is the lattice spacing small enough?, Phys. Rev. D **106**, 054503 (2022), arXiv:2204.12256 [hep-lat].
- [36] G. Wang, T. Draper, K.-F. Liu, and Y.-B. Yang (chiQCD), Muon  $g-2$  with overlap valence fermion, (2022), arXiv:2204.01280 [hep-lat].
- [37] M. Cè *et al.*, Window observable for the hadronic vacuum polarization contribution to the muon  $g - 2$  from lattice QCD, (2022), arXiv:2206.06582 [hep-lat].
- [38] C. Alexandrou *et al.*, Lattice calculation of the short and intermediate time-distance hadronic vacuum polarization contributions to the muon magnetic moment using twisted-mass fermions, (2022), arXiv:2206.15084 [hep-lat].
- [39] A. Bazavov *et al.*, Light-quark connected intermediate-window contributions to the muon  $g-2$  hadronic vacuum polarization from lattice QCD, (2023), arXiv:2301.08274 [hep-lat].
- [40] A. Boccaletti *et al.*, High precision calculation of the hadronic vacuum polarisation contribution to the muon anomaly, (2024), arXiv:2407.10913 [hep-lat].
- [41] S. Kuberski, M. Cè, G. von Hippel, H. B. Meyer, K. Ottnad, A. Risch, and H. Wittig, Hadronic vacuum polarization in the muon  $g - 2$ : the short-distance contribution from lattice QCD, JHEP **03**, 172, arXiv:2401.11895 [hep-lat].
- [42] S. Spiegel and C. Lehner, A high-precision continuum limit study of the HVP short-distance window, (2024), arXiv:2410.17053 [hep-lat].
- [43] C. Lehner *et al.*, Status of the RBC/UKQCD HVP program (2024), the 41st International Symposium on Lattice Field Theory. <https://conference.ippp.dur.ac.uk/event/1265/contributions/7454/attachments/5725/7497/talk.pdf>.
- [44] M. Bruno, T. Izubuchi, C. Lehner, and A. S. Meyer, Exclusive Channel Study of the Muon HVP, PoS **LATTICE2019**, 239 (2019), arXiv:1910.11745 [hep-lat].
- [45] M. Della Morte *et al.*, A lattice calculation of the hadronic vacuum polarization contribution to  $(g - 2)_\mu$ , EPJ Web Conf. **175**, 06031 (2018), arXiv:1710.10072 [hep-lat].
- [46] D. Bernecker and H. B. Meyer, Vector Correlators in Lattice QCD: Methods and applications, Eur. Phys. J. **A47**, 148 (2011), arXiv:1107.4388 [hep-lat].
- [47] T. Blum, T. Izubuchi, and E. Shintani, New class of variance-reduction techniques using lattice symmetries, Phys. Rev. D **88**, 094503 (2013), arXiv:1208.4349 [hep-lat].
- [48] E. Shintani, R. Arthur, T. Blum, T. Izubuchi, C. Jung, and C. Lehner, Covariant approximation averaging, Phys. Rev. D **91**, 114511 (2015), arXiv:1402.0244 [hep-lat].
- [49] M. A. Clark, C. Jung, and C. Lehner, Multi-Grid Lanczos, in *35th International Symposium on Lattice Field Theory (Lattice 2017) Granada, Spain, June 18-24, 2017* (2017) arXiv:1710.06884 [hep-lat].
- [50] M. Peardon, J. Bulava, J. Foley, C. Morningstar, J. Dudek, R. G. Edwards, B. Joo, H.-W. Lin, D. G. Richards, and K. J. Juge (Hadron Spectrum), A Novel quark-field creation operator construction for hadronic physics in lattice QCD, Phys. Rev. D **80**, 054506 (2009), arXiv:0905.2160 [hep-lat].
- [51] M. Bruno, D. Hoying, T. Izubuchi, C. Lehner, A. S. Meyer, and M. Tomii, Isospin 0 and 2 two-pion scattering at physical pion mass using distillation with periodic boundary conditions in lattice QCD, (2023), arXiv:2304.03313 [hep-lat].
- [52] C. Lehner *et al.*, Grid Python Toolkit (GPT).
- [53] R. C. Brower, H. Neff, and K. Orginos, The Möbius domain wall fermion algorithm, Comput. Phys. Commun. **220**, 1 (2017), arXiv:1206.5214 [hep-lat].
- [54] Y. Shamir, Chiral fermions from lattice boundaries, Nucl. Phys. B **406**, 90 (1993), arXiv:hep-lat/9303005.
- [55] V. Furman and Y. Shamir, Axial symmetries in lattice QCD with Kaplan fermions, Nucl. Phys. B **439**, 54 (1995), arXiv:hep-lat/9405004.
- [56] T. Blum *et al.* (RBC, UKQCD), Domain wall QCD with physical quark masses, Phys. Rev. D **93**, 074505 (2016), arXiv:1411.7017 [hep-lat].
- [57] M. Luscher and U. Wolff, How to Calculate the Elastic Scattering Matrix in Two-dimensional Quantum Field Theories by Numerical Simulation, Nucl. Phys. B **339**, 222 (1990).
- [58] B. Blossier, M. Della Morte, G. von Hippel, T. Mendes, and R. Sommer, On the generalized eigenvalue method for energies and matrix elements in lattice field theory, JHEP **04**, 094, arXiv:0902.1265 [hep-lat].
- [59] G. M. de Divitiis, R. Frezzotti, V. Lubicz, G. Martinelli, R. Petronzio, G. C. Rossi, F. Sanfilippo, S. Simula, and N. Tantalo (RM123), Leading isospin breaking effects on the lattice, Phys. Rev. D **87**, 114505 (2013), arXiv:1303.4896 [hep-lat].

- [60] P. Boyle, V. Gülpers, J. Harrison, A. Jüttner, C. Lehner, A. Portelli, and C. T. Sachrajda, Isospin breaking corrections to meson masses and the hadronic vacuum polarization: a comparative study, *JHEP* **09**, 153, arXiv:1706.05293 [hep-lat].
- [61] D. Giusti, V. Lubicz, G. Martinelli, F. Sanfilippo, and S. Simula, Electromagnetic and strong isospin-breaking corrections to the muon  $g - 2$  from Lattice QCD+QED, *Phys. Rev. D* **99**, 114502 (2019), arXiv:1901.10462 [hep-lat].
- [62] M. Di Carlo, D. Giusti, V. Lubicz, G. Martinelli, C. T. Sachrajda, F. Sanfilippo, S. Simula, and N. Tantalo, Light-meson leptonic decay rates in lattice QCD+QED, *Phys. Rev. D* **100**, 034514 (2019), arXiv:1904.08731 [hep-lat].
- [63] P. Boyle *et al.*, Isospin-breaking corrections to light-meson leptonic decays from lattice simulations at physical quark masses, (2022), arXiv:2211.12865 [hep-lat].
- [64] M. T. Hansen and A. Patella, Finite-volume effects in  $(g - 2)_\mu^{\text{HVP,LO}}$ , *Phys. Rev. Lett.* **123**, 172001 (2019), arXiv:1904.10010 [hep-lat].
- [65] M. T. Hansen and A. Patella, Finite-volume and thermal effects in the leading-HVP contribution to muonic  $(g - 2)$ , *JHEP* **10**, 029, arXiv:2004.03935 [hep-lat].
- [66] H. Akaike, A new look at the statistical model identification, *IEEE Trans. Automatic Control* **19**, 716 (1974).
- [67] G. E. Benton, D. Boito, A. Keshavarzi, K. Maltman, S. Peris, and M. Golterman, (2024), private communication.
- [68] D. Giusti, F. Sanfilippo, and S. Simula, Light-quark contribution to the leading hadronic vacuum polarization term of the muon  $g - 2$  from twisted-mass fermions, *Phys. Rev. D* **98**, 114504 (2018), arXiv:1808.00887 [hep-lat].
- [69] E. Shintani and Y. Kuramashi (PACS), Hadronic vacuum polarization contribution to the muon  $g - 2$  with 2+1 flavor lattice QCD on a larger than  $(10 \text{ fm})^4$  lattice at the physical point, *Phys. Rev. D* **100**, 034517 (2019), arXiv:1902.00885 [hep-lat].
- [70] C. T. H. Davies *et al.* (Fermilab Lattice, LATTICE-HPQCD, MILC), Hadronic-vacuum-polarization contribution to the muon's anomalous magnetic moment from four-flavor lattice QCD, *Phys. Rev. D* **101**, 034512 (2020), arXiv:1902.04223 [hep-lat].
- [71] A. Gérardin, M. Cè, G. von Hippel, B. Hörz, H. B. Meyer, D. Mohler, K. Ottnad, J. Wilhelm, and H. Wittig, The leading hadronic contribution to  $(g - 2)_\mu$  from lattice QCD with  $N_f = 2 + 1$  flavours of  $\mathcal{O}(a)$  improved Wilson quarks, *Phys. Rev. D* **100**, 014510 (2019), arXiv:1904.03120 [hep-lat].
- [72] D. Giusti and S. Simula, Lepton anomalous magnetic moments in Lattice QCD+QED, *PoS LATTICE2019*, 104 (2019), arXiv:1910.03874 [hep-lat].
- [73] D. Boito, M. Golterman, K. Maltman, and S. Peris, Data-based determination of the isospin-limit light-quark-connected contribution to the anomalous magnetic moment of the muon, *Phys. Rev. D* **107**, 074001 (2023), arXiv:2211.11055 [hep-ph].
- [74] We note that after the unblinding of our result at Lattice 2024 in July of 2024, at the KEK workshop of the Muon  $g-2$  Theory Initiative in September of 2024 unblinded results for  $a_\mu^{\text{LD,iso,conn,ud}}$  and  $a_\mu^{\text{iso,conn,ud}}$  were presented by the Mainz collaboration. At the point of finalizing this manuscript the Mainz result had not yet appeared in the literature.
- [75] P.A. Boyle *et al.*, Grid.
- [76] C. Jung *et al.*, Columbia Physics System (CPS).
- [77] M. Bruno, pyobs (2023).



## SUPPLEMENTAL MATERIAL

## Model averaging

### Test of the finite-volume corrections

In Fig. 6, we provide additional details about the excellent agreement of the Hansen-Patella formalism [64, 65] with the observed behavior in the lattice data for both physical pion mass and up to  $m_\pi \approx 280$  MeV. We use the monopole ansatz and vary the resonance mass parameter from  $m_\rho = 727$  to 770 MeV to generate the uncertainty estimates. Remarkably, the lattice data agrees for fixed Euclidean time  $t$  in all studied cases very well with the Hansen-Patella results. Our study extends from  $m_\pi L \approx 4$  to  $m_\pi L \approx 8$  for which the finite-volume corrections are smaller than the statistical uncertainties of the lattice result.

### Distinct features of individual analysis groups

In the following, we summarize the main distinct features of the individual analysis groups that were identified during the relative unblinding:

- Group A provided a lattice spacing determination that was already used in Ref. [31].
- Group B provided an independent lattice spacing determination, which did not include an ansatz of  $w_0 = w_0^{\text{cont}} + a^2 w_0^{\text{slope}}$  constraining the continuum extrapolation of  $w_0$  in the global fit. This effect is responsible for the larger statistical noise of group B compared to group A.
- Groups A and B implement model averaging and compared flat and AIC weights with consistent results. More details are provided in the following section.
- Comparing group C and group A, there are three positive  $1\sigma$  standard deviation shifts for ensembles 48I, C, and D for group C's analysis compared to group A. If group A adds these shifts to the analysis, the results of groups A and C can be brought into exact agreement. Group C did not propagate the lattice spacing uncertainty for ensembles C, D, 4, 1, 3, 9, L, which is the reason for the smaller uncertainties compared to group A.
- Group D used a third independent lattice spacing determination from a global fit. The lattice parameters are in good agreement with the results of group A.

We also provide an example of the cross-checks that were performed prior to relative unblinding in Fig. 7.

The individual fit results described in the main text of the manuscript for the RBC/UKQCD24 prescription are shown in Fig. 8. We note that the variation of the fits is of the size of the statistical uncertainties. Fits that include a pion mass curvature term are preferred, however, the p-value of fits using a linear pion mass dependence is not negligible.

We perform model averaging by considering a probability  $P(M|D)$  of a given model  $M$  given the data  $D$  that is either given by the AIC, a  $\chi^2$  term only, or a flat weight of constant  $P(M|D)$ . For the AIC, we use

$$P(M|D) \propto e^{-\frac{1}{2}\chi^2 - k} \quad (9)$$

with number of fit parameters  $k$  and the proportionality constant chosen such that  $\sum_M P(M|D) = 1$ . Expectation values of functions  $f$  of common parameters  $p$  are defined by

$$\langle f(p) \rangle = \sum_M \langle f(p) \rangle_M P(M|D), \quad (10)$$

where  $\langle \cdot \rangle_M$  is the expectation value within a model  $M$ . The total variance of  $f(p)$  is

$$\begin{aligned} & \langle f(p)^2 \rangle - \langle f(p) \rangle^2 \quad (11) \\ &= \sum_M \langle f(p)^2 \rangle_M P(M|D) - \left( \sum_M \langle f(p) \rangle_M P(M|D) \right)^2 \\ &= \sum_M \sigma_{f(p),M}^2 P(M|D) \\ &+ \sum_M \langle f(p) \rangle_M^2 P(M|D) - \left( \sum_M \langle f(p) \rangle_M P(M|D) \right)^2 \end{aligned}$$

with

$$\sigma_{f(p),M}^2 = \langle f(p)^2 \rangle_M - \langle f(p) \rangle_M^2. \quad (12)$$

When quoting uncertainties from the model averaging procedure we quote the first line

$$\sigma_{f(p),\text{stat}}^2 = \sum_M \sigma_{f(p),M}^2 P(M|D) \quad (13)$$

as the statistical variance and the second line

$$\begin{aligned} \sigma_{f(p),\text{sys}}^2 &= \sum_M \langle f(p) \rangle_M^2 P(M|D) \\ &- \left( \sum_M \langle f(p) \rangle_M P(M|D) \right)^2 \quad (14) \end{aligned}$$

as the systematic variance. By construction the statistical and systematic variance add to the total. We show in Fig. 9 that the results are largely independent of the specific choice of  $P(M|D)$ .

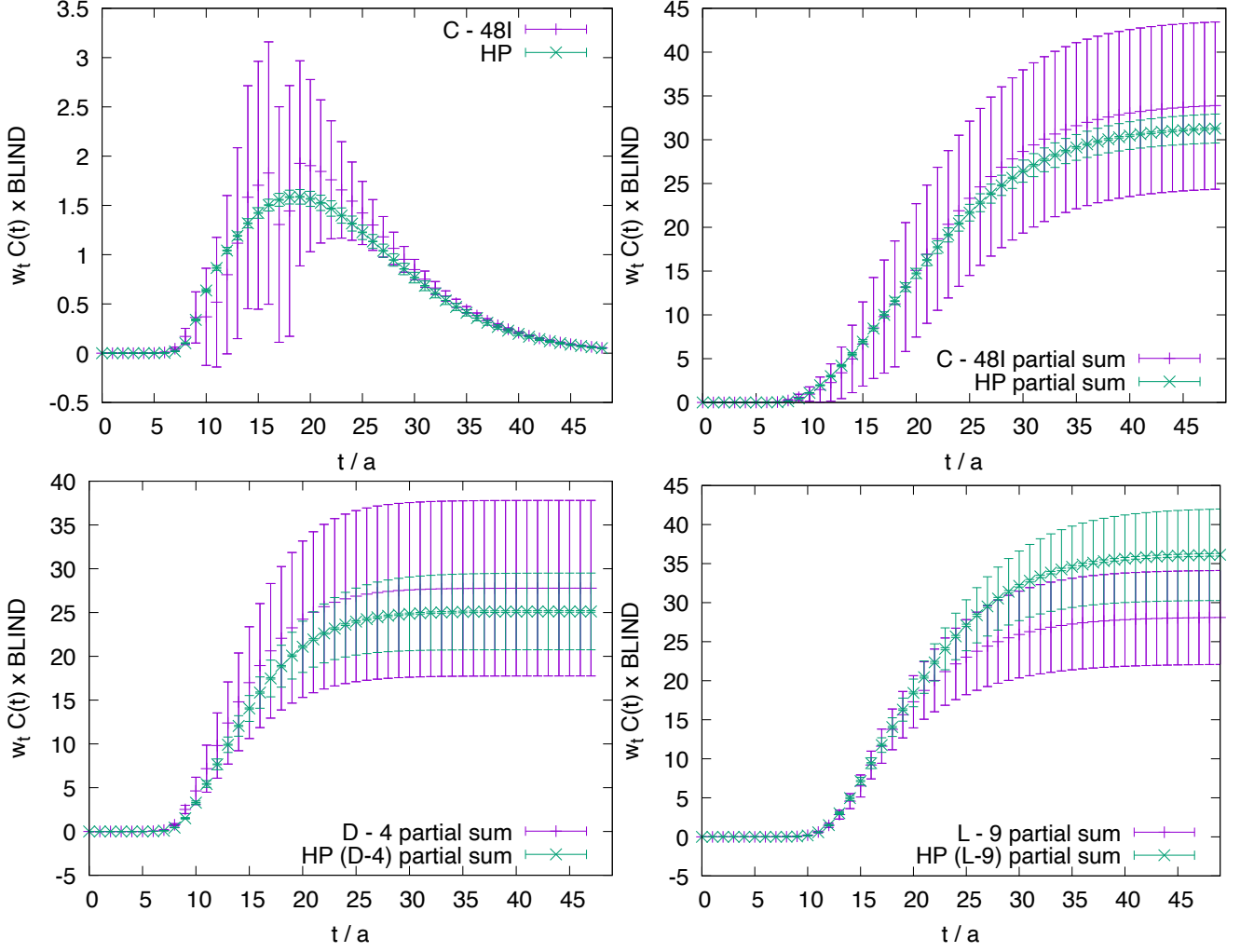


FIG. 6. We show the difference of ensemble pairs in the time-momentum representation which only differ by the lattice volume and compare the result to the Hansen-Patella formalism in the monopole ansatz. In the top left panel, we show the integrand for ensembles C and 48I at physical pion mass and in the top right panel, we show the partial sum  $\sum_{t'=0}^t w_{t'} C(t')$  for the same ensembles. The bottom row shows the partial sums of the integrands for ensembles with pion mass approximately equal to 280 MeV from  $m_\pi L \approx 4$  to  $m_\pi L \approx 8$ .

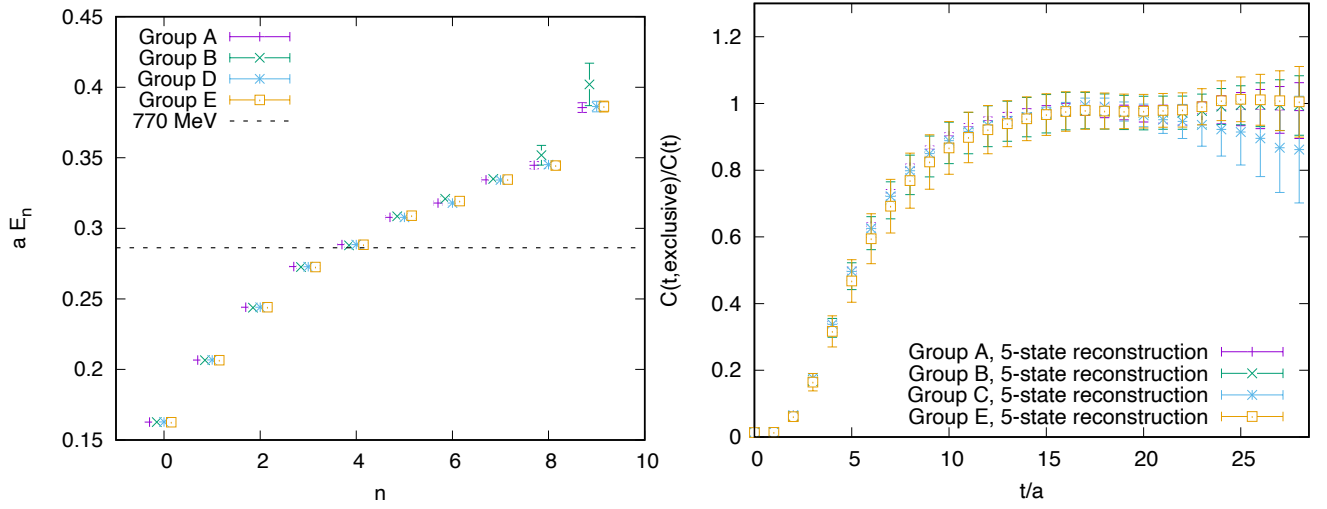


FIG. 7. Cross-checks of quantities that are not affected by the blinding factor. In the left panel we show the check of the spectrum of ensemble 96I and in the right panel we show the ratio of  $C^5(t)/C(t)$  for the 64I ensemble as performed by the different groups.

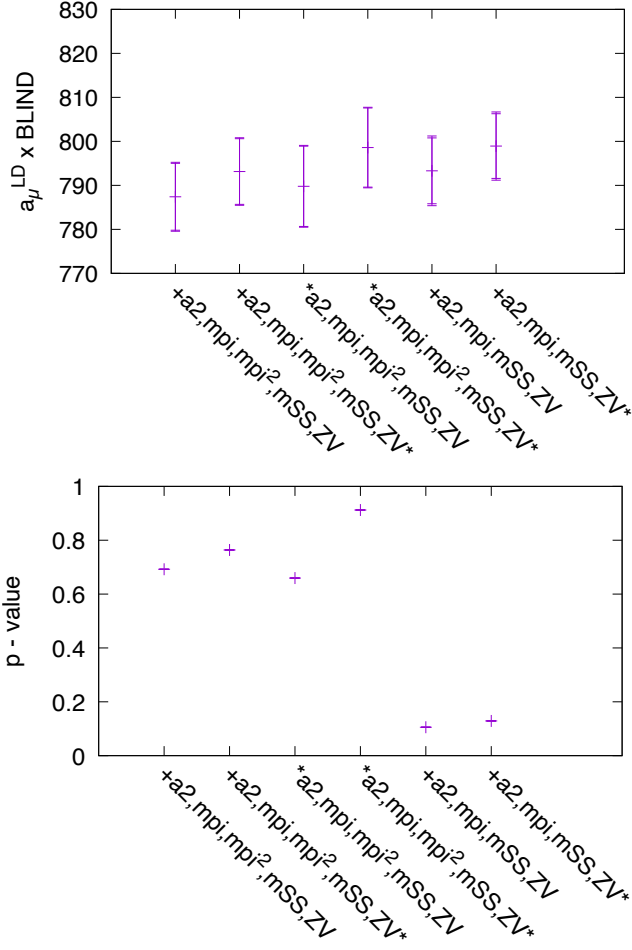


FIG. 8. Result of the individual fits of the RBC/UKQCD24 prescription in the BMW20 world. The  $f_+$  fits are denoted as  $+a^2$ , the  $f_*$  fits are denoted as  $*a^2$ . The fits with  $f_3 = 0$  are denoted by the absence of the  $\text{mpi}^2$  term. The fits using  $Z_V^\pi$  are denoted by ZV and the fits using  $Z_V^*$  are denoted by ZV\*. The top panel shows the fit results and the bottom panel shows the corresponding p-values.

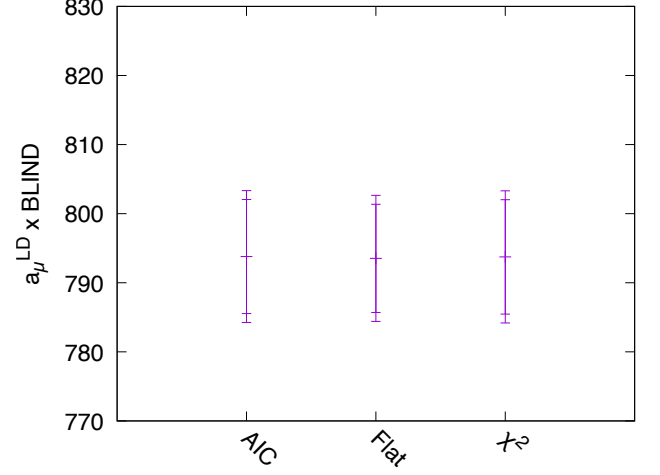


FIG. 9. We show the final fit results in the RBC/UKQCD24 prescription in the BMW20 world for different model probabilities  $P(M|D)$  in the model averaging procedure.